Asociación Argentina
de Mecánica Computacional

Mecánica Computacional Vol XXVII, págs. 1305-1324 (artículo completo)
Alberto Cardona, Mario Storti, Carlos Zuppa. (Eds.)
San Luis, Argentina, 10-13 Noviembre 2008

BOUNDARY ELEMENT ANALYSIS OF THREE-DIMENSIONAL INTERFACE CRACKS IN A TRANSVERSELY ISOTROPIC BIMATERIAL USING THE ENERGY DOMAIN INTEGRAL.

Nicolás O. Larrosa[a], Jhonny E. Ortiz[b], Adrián P. Cisilino[a]

[a]Department of Mechanical Engineering, Welding and Fracture Division – INTEMA - CONICET
Universidad Nacional de Mar del Plata, Av. Juan B. Justo 4302, (7600) Mar del Plata, Argentina
[b]School of Engineering, University of Seville, Camino de los descubrimientos s/n, Sevilla, e-41092

Keywords: Three-dimensional interface cracks, dissimilar transversely isotropic bimaterial, Energy Domain integral, Boundary element method

Abstract: A general multidomain boundary element analysis of the thee-dimensional interface crack problem for dissimilar transversely isotropic materials is presented in the present publication. The Energy Domain Integral (EDI) methodology is used to compute the J-integral. Different examples are solved to demonstrate the capability of the method. Some of them are benchmark examples that were used to validate the BEM code and the other ones are examples that are considered interesting by the authors for their technological application.

1 INTRODUCTION

Composites usage for structural porpoise in engineering and civil applications has been growth in a very high rate in the last 15 years. The main reason of this statement is the property of these materials to offer “customized” behaviors and the improvement of composite manufacture.

Fracture-Mechanics should be able to predict a certain way of behavior during the material life time, in order to achieve minimum levels of safety and reliability and to be of massive use.

Transversely isotropic materials are those with an axis of symmetry such that all directions perpendicular to the axis is a plane of isotropy. Many fiber-reinforced composites show this kind of behavior from a macroscopic point of view. Among others, fracture mechanical characterization of three dimensional transversely isotropic materials was reported by Sáez, Ariza and Dominguez (1997) and by Ariza and Dominguez (2003) .

Interface Crack propagation between dissimilar materials is a typical failure mechanisms in composites. For example, the macroscopic behavior of unidirectional fiber-reinforced-composite materials is strongly dependent on the strength of the fiber/matrix adhesion. The stress concentrations around the fibers lead to micro-crack initiation, which will grow along a ply to become a complete transverse crack.

Once cracking initiation has arisen, preventing crack growth (propagation) is the variable to control in order the keep the material in a reliable condition.

One of the most widely used parameters to characterize fracture-mechanical behavior is the *J*-integral, developed by Rice (1968). It characterizes the crack driving force for two-dimensional problems. Therefore, for general three-dimensional cases involving cracks of arbitrary shape an alternative form for the *J*-integral is needed.

Being an energy approach, the *J*-integral eliminates the need to solve local crack tip fields accurately, since if the integration domain is defined over a relatively large portion of the mesh, an accurate modeling of the crack tip is unnecessary because the crack tip fields contribution to J are not significant.

Three basic schemes have evolved for the numerical computation of the J-integral in three dimensions: virtual crack extension methods (Hellen, T.K, 1975; Parks, D.M, 1974), generalization of Rice’s contour integral (Carpenter W.C., Read D.T. and Dodds R.H., 1986), and domain integral methods (Moran B. and Shih C.F, 1987 ; Nikishkov G.P. and Atluri S.N, 1987 ; Saliva R., Vénere M.J., Padra C., Taroco E. and Feijoo R., 2000).

Domain integrals are equivalent to the virtual crack extension technique and are better suited for numerical analysis than contour integral methods (it is difficult to evaluate stresses and strains along a vanishing small contour). Previous work by one of the authors of this paper has proved the versatility and efficiency of the EDI in the three-dimensional BEM analysis of isotropic cracked bodies (Cisilino A.P., Aliabadi M.H., and Otegui J.L , 1998 ; Cisilino A.P. and Aliabadi M.H 1999).This works aims to be a continuation of that done by Cisilino and Ortiz (2005) being more general allowing the bimaterial to be made of transversely isotropic solids.

The EDI, which is derived applying the divergence theorem to Rice's *J*-integral, was chosen for this work. It produces an integral defined over a finite volume enclosing some portion of the crack front.

In this work, the EDI computation for an interface crack for dissimilar three-dimensional transversely isotropic materials is presented. It can be shown that the EDI is independent of the integration volume, analogous to Rice's *J*-integral, and it can be interpreted as the energy

released per unit of segment of crack advanced, equal to the potential energy diminution. To develop the domain integral, the EDI incorporates an auxiliary function *q*, which can be interpreted as a virtual crack-front advance, but has the advantage that only one computer run is necessary to evaluate the point-wise energy release rate along the complete crack front.

The implementation of the EDI requires nodal values of tension, displacements and displacements gradients within the integration contour that enclosures each segment of the crack front. The Boundary Element Method (BEM) is a technique that permits the computing of the forenamed unknowns. The BEM is particularly efficient for crack problems due to its ability to model high stress gradients like those occurring near the crack tip. As BEM produces more accurate stresses and strains at internal points (compared to other numerical techniques), better results for EDI can be achieved.

In this case, it has been used the multi-region BEM, that considers the problem of a multi-material domain. Quadrilateral Lagrange elements with nine nodes were used to mesh the contour, except in the bimaterial interface surface, where one and two semi-discontinues side elements were implemented to avoid common nodes in the bimaterial intersection.

Once the multi-region BEM analysis has been done, the nodal analytical values at the interior points are known, computed using formulations that relates the boundary solutions to source points at the domain.

The contour mesh of the body surface with boundary elements around the crack front has been design in a “spider-web” shape. This was done in order to build the integration volumes to compute the EDI, adopting the shape of cylinders, each one made of cells. The cells are similar to the three-dimensional finite elements of 27 nodes and are implemented in an isoparametric interpolation scheme, being their nodes the internal points of the BEM analysis. Values of stress, strains and displacements gradients were approximated at the cells using the information known for these internal points.

The EDI computation was repeated for every position of the crack front in order to know how it varies over the crack front.

Finally, several benchmark examples were tested in order to validate the tool and afterwards other problems of industrial and R&D interest were solved.

2 TRANSVERSELY ISOTROPIC MATERIALS

It is worth reviewing the basic relations governing the behavior of a transversely isotropic material (Love, A.E.H.A, 1944; T. C. T. Ting, 1996).

The equilibrium equation for a general linearly elastic material with no body forces in three dimensions are:

$$\sigma_{ij},_{j} = 0 \tag{1}$$

Under small displacements, the strains can be written as the Cauchy infinitesimal strain tensor:

$$\varepsilon_{ij} = \frac{1}{2}\left(u_{i,j} + u_{j,i}\right) \tag{2}$$

The strain-displacement equation 2 represents a system of six independent equations relating the six strain components to the three displacement components.

The stress-strain relationship is

$$\sigma_{ij} = C_{ijks}\varepsilon_{ks} \tag{3}$$

C_{ijks} are the elastic constants. There are 81 possible constants in equation 3 but only 21 are independent. This is the case of an anisotropic material. For transversely isotropic materials in which the axis of symmetry coincides with a Cartesian axis, for example, the x_3 axis, the stress-strain relation can be written in terms of five independent constants in the following matrix form:

$$\begin{Bmatrix} \sigma_{11} \\ \sigma_{22} \\ \sigma_{33} \\ \sigma_{12} \\ \sigma_{13} \\ \sigma_{23} \end{Bmatrix} = \begin{Bmatrix} C_{11} & C_{12} & C_{13} & 0 & 0 & 0 \\ C_{12} & C_{11} & C_{13} & 0 & 0 & 0 \\ C_{13} & C_{13} & C_{33} & 0 & 0 & 0 \\ 0 & 0 & 0 & \frac{(C_{11}-C_{12})}{2} & 0 & 0 \\ 0 & 0 & 0 & 0 & C_{66} & 0 \\ 0 & 0 & 0 & 0 & 0 & C_{66} \end{Bmatrix} \begin{Bmatrix} \varepsilon_{11} \\ \varepsilon_{22} \\ \varepsilon_{33} \\ 2\varepsilon_{12} \\ 2\varepsilon_{13} \\ 2\varepsilon_{23} \end{Bmatrix} \tag{4}$$

Being:

$$C_{11} = \frac{E(n-\nu'^2)}{\lambda(1+\nu)};\ C_{12} = \frac{E(n+\nu'^2)}{\lambda(1+\nu)};\ C_{13} = \frac{E\nu'}{\lambda};\ C_{33} = \frac{E(1-\nu)}{\lambda};\ C_{66} = \mu' \tag{5}$$

$$\lambda = n(1-\nu) - 2\nu'^2; n = \frac{E}{E'} \tag{6}$$

Where

1. E and E' are the Young's moduli in the plane of isotropy and in the directions normal to it, respectively.
2. ν is the Poisson's ratio that represents the strain response in the plane of isotropy due to an action parallel to it. Besides, ν' represents the lateral strain response for the planes normal to the plane of isotropy.
3. μ' is the shear modulus for the planes normal to the planes of transverse isotropy.

C_{ij} are the elastic constants in a condensed notation in terms of only two subindices.

Isotropic materials are a particular case of transversely isotropic materials. It can be observe by replacing the following values in equation 4:

$$C_{11} = C_{33} = \lambda + 2\mu;\ C_{12} = C_{13} = \lambda;\ C_{44} = C_{66} = \mu \tag{7}$$

3 THE ENERGY DOMAIN INTEGRAL (EDI)

Consider a three-dimensional crack front with a continuously turning tangent as depicted in Figure 1a. Define a local coordinate system x^* at position η, where the crack energy release rate is evaluated, given by x_1^* normal to the crack front, x_2^* normal to the crack plane, and tangent x_2^* to the crack front

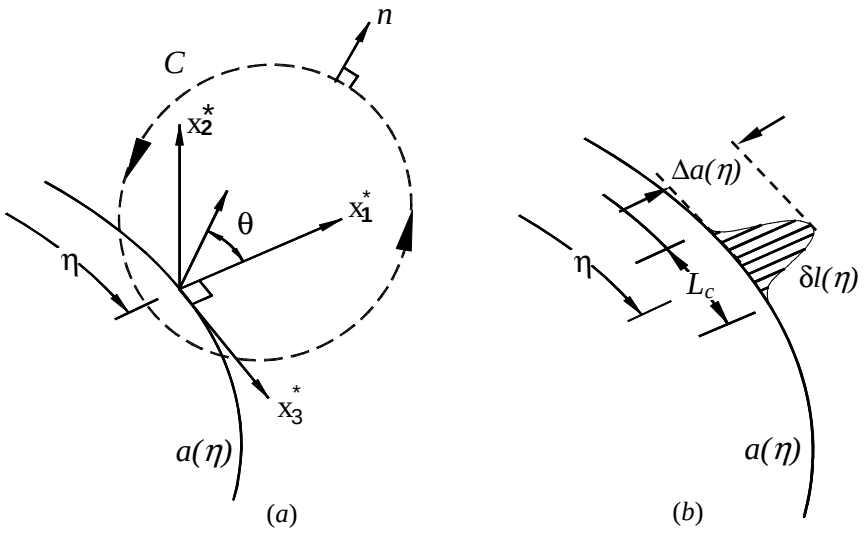

Figure 1: (a) Definition of the local orthogonal Cartesian coordinates at point η on the crack front, (b) Virtual crack front advance.

Following Natha and Moran (1993), the general crack-tip contour integral along three-dimensional crack front takes the form (Figure 1)

$$I(\eta)=\lim_{C\to 0}\delta l(\eta)\int_{C(\eta)}\left(w\cdot\delta_{kj}-\sigma_{ij}^{*}u_{i,k}^{*}\right)n_j dC \tag{8}$$

where w is the strain energy density, σ_{ij}^{*} and $u_{i,k}^{*}$ are Cartesian components of stress and displacement derivatives expressed in the local system x^{*},δl is the local crack extension, n_j is the unit vector normal to the contour C (which lies in the x_1^{*}-x_2^{*} plane), and $dC(\eta)$ is the differential of the arc length C (Figure 1 a). It is worth noting that, although equation 8 comes from a two-dimensional analysis, it applies for the three-dimensional case, as in the limit as $C\to 0$, plain strain conditions prevail so that three-dimensional fields approach the plane problem.

In order to derive the equivalent domain representation of equation 8 we consider a small segment L_c of the crack front that lies in the local x_1^{*}-x_3^{*} plane as shown in Figure 1 b. Next we assume that the segment undergoes a virtual crack advance in the plane of the crack, and we define the magnitude of the advance at each point η as $\Delta a(\eta)$. We note that $\Delta a(\eta)$ varies continuously along L_c and vanishes at each end of the segment. Now let:

$$\bar{I}=\int_{L_C} I(\eta)\Delta a(\eta)d\eta \tag{9}$$

where $I(\eta)$ is the integral defined in equation 8.When $I(\eta)$ belongs to the point-wise energy release rate, equation 9 gives the total energy released when the finite segment L_c undergoes the virtual crack advance.

The appropriate domain form of the pointwise crack-tip contour integral can be obtained from equation 9 by considering a tubular domain V surrounding the crack segment (Figure 2).

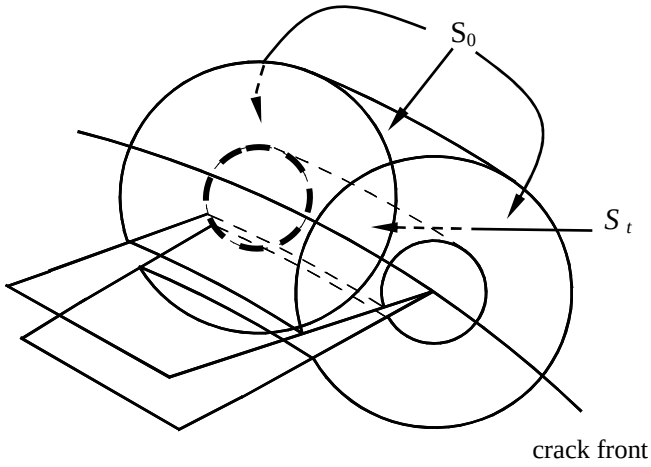

Figure 2: Tubular domain surrounding a segment of the crack front

As shown in Figure 2, the surface S_t is formed by translating the contour C along the segment L_c, and S_o stands for the outer surface of V including the ends. Next an auxiliary function q is introduced, which is sufficiently smooth in V and it is defined on the surfaces of V as follows:

$$q = \begin{cases} \Delta a(\eta) \cdot \delta l(\eta) & \text{on } S_t \\ 0 & \text{on } S_o. \end{cases} \tag{10}$$

Finally, in the limit as the tubular surface S_t is shrunk onto the crack segment L_c; and in the absence of crack face tractions, we obtain the domain integral:

$$\bar{I} = \int_V \left(\sigma_{ij}^* u_{j,k}^* - w\delta_{ki} \right) q_{,i} dV. \tag{11}$$

In the evaluation of the energy release rate, in the absence of body forces the integral given by equation 11 reduces to the domain representation of the familiar J-integral. A simple relationship between $J(\eta)$ and the point-wise crack-tip integral $I(\eta)$ can be obtained if it is assumed that $I(\eta)$ is constant along the segment L_c. It follows directly from equation 9) that:

$$J(\eta) = \frac{\bar{I}}{\int_{L_c} \Delta a(\eta) d\eta} \tag{12}$$

4 BOUNDARY ELEMENT ANALYSIS

The computation of the J-integral was implemented in the BEM code as a post-processing procedure, and so it could be applied to the results from a particular model at a later stage. In order to account for the different material properties at both sides of the crack, a multiple domain BEM formulation was used, as shown in Figure 3. The BEM formulation follows standard procedures, for which the equilibrium and continuity conditions are enforced at the common interface between the domains (Brebbia C.A., Telles J.L.F, and Wrobel, L.C, 1984).

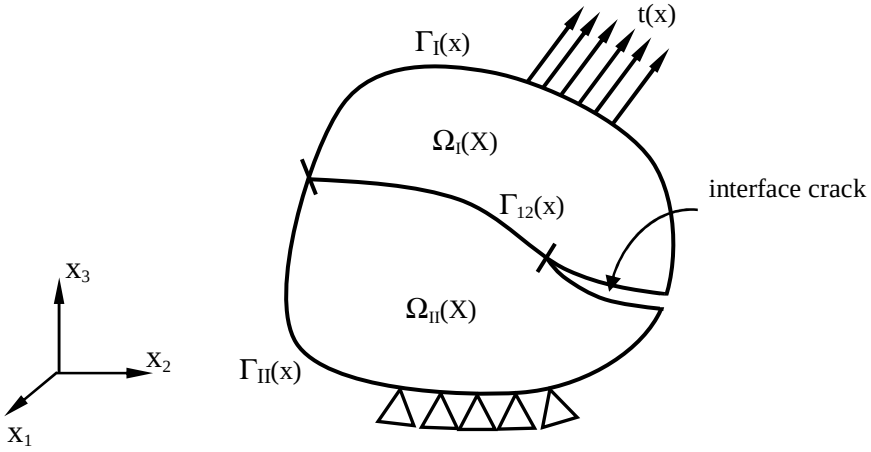

Figure 3: Schematic representation of the multidomain technique for a non-homogeneous body.

The solution of a unit point force applied at the interior of an infinite transversely isotropic three-dimensional material was studied by many authors. The solutions provided have the deficiency of being expressed in a different way depending on the conditions satisfied by the elastic constants. However, Y.C Pan and T.W Chou (1976), unlike previous publications, obtained 'a unified solution which is applicable for all stable transversely isotropic materials'. Nevertheless, M. Loloi (2000) found that these solutions had never been reported in the literature. Later, he found that they were not in a suitable form for use in the boundary integral equation technique. He provided the suitable form of the fundamental solutions convenient for use in the boundary integral equation method (See Appendix). This approach is used in the present work.

4.1 Displacement derivatives, stresses and strains

4.1.1 Internal Points

As has been stated in Section 3, the computation of the *J*-integral requires the stress and displacement derivative fields σ_{ij}^{*} and $u_{i,k}^{*}$ to be known within the integration volume *V*. Although these quantities must be expressed in the local crack-front coordinate system x^{*}, in this work, and for the sake of simplicity, they will be firstly computed in the global system *x* and later transformed to the local system x^{*}. Bearing this in mind, and in order to integrate the computation of the *J*-integral into the BEM formulation, derivatives of the displacements at internal points *X´* are obtained from their boundary integral representations. The integral equation for the displacement derivatives results from the analytical differentiation of the well-known displacement boundary integral equation for a point *X'* located in the model domain

$$u_{i,m}(X') = \int_{\Gamma} U_{ij,m}^{*}(X',x)t(x)d\Gamma(x) - \int_{\Gamma} T_{ij,m}^{*}(X',x)u(x)d\Gamma(x) \tag{13}$$

where the terms $U_{ij,m}^{*}$ and $T_{ij,m}^{*}$ are the derivatives of the fundamental displacement U_{ij}^{*}, and traction T_{ij}^{*} solutions, and the boundary Γ corresponds to that of the zone where the point *X'* lies on. The corresponding expressions for the fundamental solutions U_{ij}^{*} and T_{ij}^{*} are the same obtained by Pan and Chou and are given in the Appendix.

Once the displacement derivatives $u_{i,m}$ are known, stresses σ_{ij} and strains ε_{ij} can be computed using the basic continuum mechanics relationships (equation 2 and equation 3)

4.1.2 Boundary Points

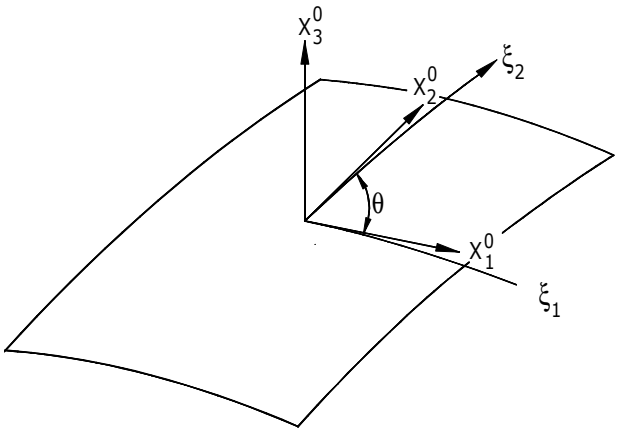

Figure 4: Local Cartesian system for boundary stress calculation.

Displacement partial derivatives $u_{i,m}$ at boundary nodes could be obtained from equation 13 by taking the limit as point *X'* moves to the boundary, *i.e. X'* $\rightarrow$ *x'*. However, this procedure is computationally expensive because of the occurrence of hypersingular integrands. In order to avoid this difficulty, stresses and strains, as well as the displacements on the model surface are evaluated in this work from the boundary displacements and tractions, following a procedure similar to that used in FEM computations. Consider with this purpose a local Cartesian system, (x_1^0, x_2^0, x_3^0) such that x_3^0 is the unit vector in the normal direction to the boundary element (see Figure 4). If u_j^0, ε_{ij}^0, σ_{ij}^0 and t_j^0 are the displacements, strains, stresses and tractions in the local system, stress components in the normal direction can be written as:

$$\sigma_{i3}^0 = t_i^0 , \qquad i=1, 2, 3. \tag{14}$$

The remaining stress tensor components, σ_{11}^0, σ_{12}^0 and σ_{22}^0 can be expressed in terms of t_3^0 and the tangential strain tensor components ε_{11}^0, ε_{12}^0 and ε_{22}^0.

$$\sigma_{11}^0 = t_3^0 + (C_{11}^0 - C_{13}^0)\cdot\varepsilon_{11}^0 + (C_{12}^0 - C_{13}^0)\cdot\varepsilon_{22}^0 + (C_{13}^0 - C_{33}^0)\cdot\varepsilon_{33}^0 \tag{15}$$

$$\sigma_{22}^0 = t_3^0 + (C_{12}^0 - C_{13}^0)\cdot\varepsilon_{11}^0 + (C_{11}^0 - C_{13}^0)\cdot\varepsilon_{22}^0 + (C_{13}^0 - C_{33}^0)\cdot\varepsilon_{33}^0 \tag{16}$$

$$\sigma_{12}^0 = (C_{11}^0 - C_{12}^0)\cdot\varepsilon_{12}^0 \tag{17}$$

$$\varepsilon_{33}^0 = \frac{t_3^0 - (C_{13}^0\cdot\varepsilon_{11}^0 + C_{12}^0\cdot\varepsilon_{22}^0)}{C_{33}^0} \tag{18}$$

Strain components ε_{ij}^{0} can be found using equation 2, now applied in the local coordinate system.

It is worth nothing that displacement derivatives in equation 2 are initially evaluated in the intrinsic element directions (ξ_1, ξ_2), since as it usual in BEM, boundary displacements are given in terms of the piecewise parametric representation (shape functions) of intrinsic coordinates:

$$u_i(\xi_1,\xi_2)=\sum_{n=1}^{N}\Phi^n(\xi_1,\xi_2)u_i^n \tag{19}$$

where Φ^n are the shape functions, u_i^n are the nodal values of the displacements, and N is the number of element nodes. From equation 19 it follows

$$\frac{\partial u_i}{\partial \xi_j}=\sum_{n=1}^{N}\frac{\partial \Phi^n}{\partial \xi_j}u_i^n\,. \tag{20}$$

Finally, the derivatives of the displacements in the global system are computed. Using chain differentiation, derivatives of the displacements in the global system, $u_{i,m}$ can be related to the derivatives of the displacements in the intrinsic boundary element directions, $\partial u_i/\partial \xi_j$ as follows:

$$\frac{\partial u_i}{\partial \xi_j}=\frac{\partial u_i}{\partial x_m}\frac{\partial x_m}{\partial \xi_j}. \tag{21}$$

where $\partial x_m/\partial \xi_j$ is the Jacobian matrix of the transformation. The nine components of the displacement derivatives $u_{i,m}$ can be retrieved by solving for each case a system of equations constructed using equation 21. For further details the reader is referred to the works by Cisilino A.P. and Aliabadi M.H(1999) or Cisilino A.P. and Ortiz J.E (2005)

4.2 Implementation

As has been stated in Section 3, equation 12 allows the computation of *J*-integral at any position η on the crack front. The evaluation of a volume integral within a domain enclosing a segment of the crack front L_c is required. A natural choice here is to make η coincident with the element nodes on the crack front, while L_c is taken as the element or element sides at which points η lies (see Figure 5). The portion of the model domain in which the volume integrals are evaluated is discretized using 27-noded isoparametric (brick) cells, over which stresses, strains and displacements derivatives are approximated by products of the cell shape functions Ψ^i and the nodal values of σ_{ij}, ε_{ij} and $u_{i,j}$. Nodal values of these variables are computed following the procedures introduced in Sections 4.2, depending on whether the node is internal or lies on the model boundary. Volume discretization is designed to have web-style geometry around the crack front, while the integration volumes are taken to coincide with the different rings of cells. This is illustrated in Figure 6, where the frontal face of the model has been partially removed to show the crack and the integration domains.

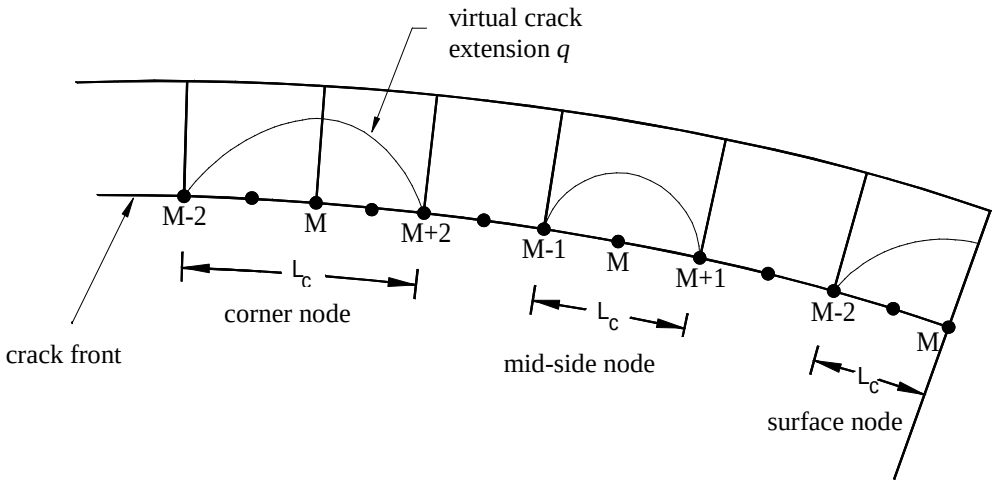

Figure 5: Schematic representation of the volume cells in the crack front region illustrating the virtual crack extensions for a corner node, a mid-node and a surface node.

As depicted in Figure 5, three different cases need to be considered, depending on whether the node of interest M is in the middle of an element side (mid-node), it is shared by two elements (corner node), or it is located coincident with the external surface (surface node). If the node M is a mid-node or surface node, L_c (the segment of the crack front over which the M_1-integral is computed) spans over one element, connecting nodes M-1, M, and M+1 and nodes M-2, M-1 and M, respectively. On the other hand, if M is a corner node, L_c spans over two elements, connecting nodes from M-2 to M+2.

The auxiliary function q was introduced in Section 3 in order to model the virtual crack front advance. Since the virtual crack advance can adopt any arbitrary shape, the only requirement for function q is to be sufficiently smooth within the integration volume V as the evaluation of the EDI requires of its differentiation (Moran B. and Shih C.F, 1987). In this work q is defined to vary quadratically in the directions tangential and normal to the crack front. Within this approach, and considering that the evaluation point η is at the middle of the crack front segment L_c, and r_0 is the radius of the integration domain, the function q is written as:

$$q(x^*) = \left| 1 - \left(\frac{x_3^*}{L_C/2} \right)^2 \right| \cdot \left[1 - \left(\frac{r}{r_0} \right)^2 \right]. \tag{22}$$

where r is the distance from the crack front in the $x_1^* - x_2^*$ plane as depicted in Figure 1.

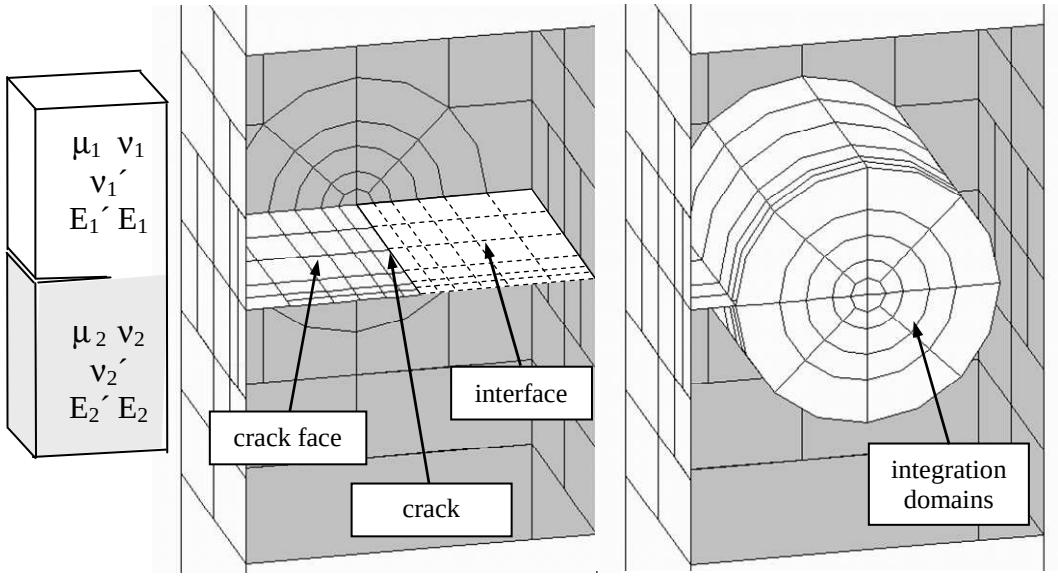

Figure 6: (a) Problem geometry, (b) Boundary Element discretization, (c) Integration domains

Although Moran and Shih [7] have shown that for the EDI the computed value of J is insensitive to the selection of the q function, it has been found that the shape of the q function is relevant for the accuracy of the computations. Note that in contrast the path independent integrals, the EDI requires of the computation of quantities at crack front vicinity to calculate the domain integral. It is well known that accuracy of computed quantities at these points is lower than at those far from the crack front. The key feature for the excellent performance of the EDI under these circumstances is the behavior of the auxiliary function q in the crack tip vicinity. Note that for the definition of q given in equation 22, the gradient $q_{,i}$ tends to zero as r tends to zero (i.e. in the vicinity of the crack front), resulting that the contribution to J of the crack front fields is not significant (see equation 11). As a consequence, the zone of the integration domain with the lowest accuracy in the results has a marginal contribution to the value of J. This fact also allows avoiding the use of quarter point or special crack tip elements to enhance the accuracy of the results in this zone. The bi-quadratic definition of q has been employed with excellent results in the computation of EDI for cracks in homogeneous materials in a previous work by one co-author of this paper. Further details and discussion on the selection of the function q can be found in a recent work by two co-authors of this paper (Cisilino A.P. and Ortiz J.E., 2004).

Function q is specified at all nodes within the integration volumes. Consistent with the isoparametric formulation, these q-values are given by:

$$q = \sum_{i=1}^{27} \Psi^i Q^i \ . \tag{23}$$

where Ψ^i are the shape functions defined within each volume cell and Q^i are the nodal values for the ith node. From the definition of q (see equation 10), $Q^i = 0$ if the ith node is on S_0, while for nodes inside V, Q^i are given by interpolating between the nodal values on L_c and S_0. Following standard manipulations:

$$q_{,j} = \sum_{i=1}^{27} \sum_{k=1}^{3} \frac{\partial \Psi^i}{\partial \zeta_k} \frac{\partial \zeta_k}{\partial x_j} Q^i \ . \tag{24}$$

where ζ_k are the coordinates in the cell isoparametric space and $\partial x_k / \partial \xi_j$ is the Jacobian matrix of the transformation.

If Gaussian integration is used, the discretized form for the *J*-integral in equation 11 is given by:

$$\bar{I} = \sum_{cells\ in\ V} \sum_{p=1}^{m} \left\{ \left(\sigma_{ij}^* u_{j,k}^* - \sigma_{ij}^* \varepsilon_{ij}^* \delta_{ki} \right) q_{,i} \det \left(\frac{\partial x_j}{\partial \zeta_k} \right) \right\}_p w_p \ . \tag{25}$$

where *m* is the number of Gaussian points per cell, and w_p are their weighting factors.

5 APPLICATION EXAMPLES: THICK CENTRE-CRACKED PANEL SPECIMEN

In this section the accuracy of BEM formulation and *J*-integral computation are assessed by considering a number of examples. The first example has two-dimensional characteristics or deal with homogeneous materials (namely the centre cracked panel (CCP)) in order to allow comparisons with results from the bibliography. Next, the CCP with transversely isotropic properties is shown, in a variety of orientations of the fibers. The former examples are compared with an ABAQUS finite element model in order to show the validity of the results, having no literature reference to compare with.

The problems analyzed possess symmetry in their geometric configuration but not in material properties, due to the transversely isotropic material nature. As a result, it was not possible to analyze only the symmetric portion of the domain by prescribing appropriate symmetry boundary conditions along the geometrical symmetry plane. Therefore, the whole model has been discretized in order to pale the non-symmetric nature of the transversely isotropic materials.

The thick CCP-specimen under Pure Mode-I solicitation was calculated. The geometry of the specimen is similar to that depicted in Figure 7 . Crack length is a=10 mm, the width $b=2a$ *and* the specimen thickness is $t=3a$.

Model discretization is depicted in Figure 6. It consists of 658 elements and 2855 nodes. Eighteen elements are placed along the crack front, and a total of 126 elements are used in the crack discretization. Four rings of cells with radii *r/a* equal to 0.1, 0.15, 0.22 and 0.32 are accommodated around the crack front for *J* computations. With this purpose 648 cells and 6438 modes are employed.

The fracture mechanical behavior of the specimen was computed for several configurations of material properties and relative zone's rotation.

First, isotropic properties were assigned to both zones (see Figure 7). Material properties are Young's Modulus E=100.000 MPa and a Poisson's ratio ν=0.3.Besides, the algorithm was run in two different possible ways, the isotropic branch and the transversely isotropic branch of the code (although isotropic material properties were consider) in order to prove the accuracy of both branches. Exactly equal results were obtained from both branches of the code.

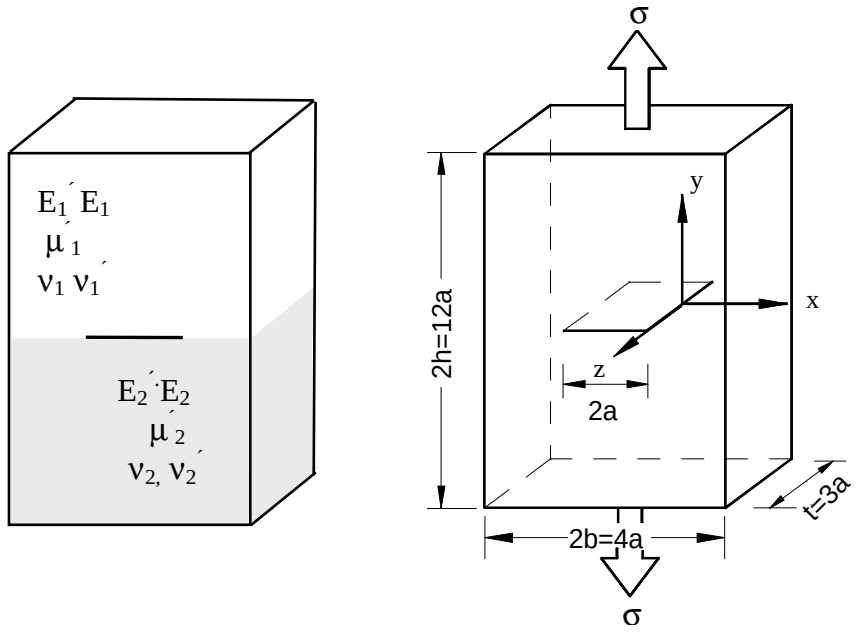

(a) *(b)*

Figure 7: *(a)* Schematic representation of the thick tension plate with a centre interface crack, *(b)* Model dimensions

The computed *J* results are compared with those from bibliography and shown in Figure 8. Results are reported over the crack front. References values are those reported by Raju, I.S. and Newman, J.C (1977) and by Cisilino (2000). Besides, a 2D FEM analysis was introduced in the comparison. All results are normalized with respect to the *J* value corresponding to the CCP specimen in plane strain condition according to Tada H., Paris P.C. and Irwin G.R (2000). The *J* value was obtained from the applied *K* value using the following expressions:

$$K = \sigma\sqrt{\pi a}\cdot F(^{a}/_{b}). \tag{26}$$

$$J = \frac{K^2}{E'}. \tag{27}$$

$$E' = \frac{E}{(1-\nu^2)}. \tag{28}$$

In equation 26, *F(a/b)* is the correction factor for *K*. The use of E' is justified in the fact that a plane strain condition is expected to prevail along most of the crack front within the domain. On the other hand, near the boundary it is expected that a thin layer will behave in a plane stress condition based on the free surface effect and $E'=E$. Thus, the *J* reference value at the free surface is computed considering both cases.

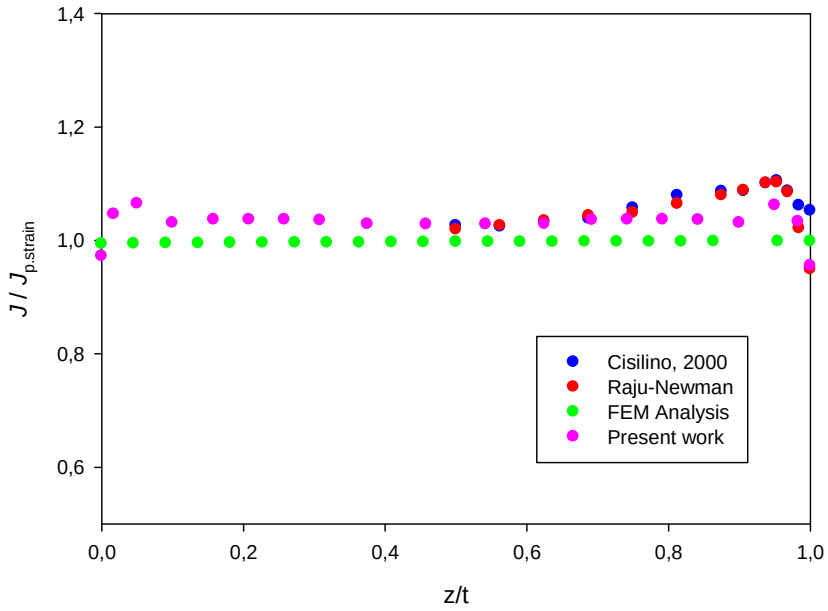

Figure 8: Normalized $J/J_{p.strain}$ values for the thick CCP specimen

Computed results and the reference values are found to have a good agreement throughout the specimen thickness as shown in Figure 8.

Second, transversely isotropic properties were assigned to the bimaterial. Several configurations were adopted in order to show the difference in the behavior of the specimen with the orientation of the fibers, and the influence of the relative orientation between the zones. Material properties used were those of a composite laminate as follows:

$$C_{ij} = \begin{Bmatrix} 5.320 & 1.340 & 3.350 & 0 & 0 & 0 \\ 1.340 & 5.320 & 3.350 & 0 & 0 & 0 \\ 3.350 & 3.350 & 251.168 & 0 & 0 & 0 \\ 0 & 0 & 0 & 1.990 & 0 & 0 \\ 0 & 0 & 0 & 0 & 5.000 & 0 \\ 0 & 0 & 0 & 0 & 0 & 5.000 \end{Bmatrix} . \quad (29)$$

Again, the results were normalized. In this case $J_{p.strain}$ was obtained by replacing in equation 26 the Young's Modulus of the plane of isotropy (C_{11}=C_{22}=5.320 MPa.). In equation 29, C_{33} represents the material strength over the perpendicular direction to the plane of isotropy. For fiber-matrix composites, the commented direction is that of the fibers. Assigning a rotation to the matrix C_{ij} we are able to rotate the plane of isotropy and change the fibers direction. In Figure 9 the convention used to distinguish the director cosines for the rotation of C_{ij} in each zones is shown. As example, if $\theta_1=\pi/2$, $\alpha_1= 0$, $\phi_1=0$ and $\theta_2=0$, $\alpha_1=\pi/2$ $\phi_2=0$, then the fibers are pointing in the x axis in Zone 1 and the y axis in Zone 2.

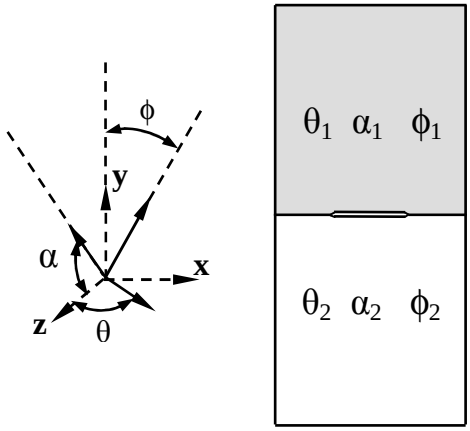

Figure 9: Director Cosines nomenclature for the bimaterial

In Figure 10, we compared the different orientations of the fibers in both zones ($\theta_1= \theta_2=\theta$, $\alpha_1= \alpha_2=\alpha$, and $\phi_1=\phi_2=\phi$). Assuming the global axis convention and the load configuration showed in Figure 7, we calculated $J/J_{p.strain}$ for the cases where the fibers coinciding with the direction of the three global axis. The examples are contrasted with a Finite Element Analysis, just to prove the accuracy of the model and to validate the formulation implemented.

As it can bee seen from Figure 10 and Table 1, good agreement with the FEM analysis is demonstrated and path independency is confirm. This can be observed in Table 1, in which for every different *r/a* value, $J/J_{p.strain}$ takes practically the same value, keeping *z/t* constant

z/t	$J/J_{p.strain}$ *r/a*				Average	FEM	Diff. %
	0,1	0,15	0,22	0,32			
0	1,1159	1,1468	1,1649	1,1870	1,1537	1,1647	-0,94%
0,017	1,1360	1,1558	1,1651	1,1697	1,1566	1,1653	-0,75%
0,033	1,1347	1,1444	1,1459	1,1402	1,1413	1,1657	-2,10%
0,458	1,1292	1,1356	1,1336	1,1242	1,1307	1,1686	-3,24%
0,5	1,1292	1,1356	1,1336	1,1242	1,1307	1,1687	-3,25%
0,542	1,1292	1,1356	1,1336	1,1242	1,1307	1,1689	-3,27%
0,583	1,1294	1,1357	1,1339	1,1247	1,1310	1,1690	-3,26%
0,95	1,1205	1,1269	1,1255	1,1175	1,1226	1,1704	-4,09%
0,967	1,1169	1,1271	1,1283	1,1212	1,1234	1,1705	-4,02%
0,983	1,1164	1,1422	1,1532	1,1507	1,1406	1,1707	-2,57%
1	1,0893	1,1377	1,1648	1,1743	1,1415	1,1712	-2,53%

Table 1: Normalized *J/Jp.strain* results for the CCP specimen when $\theta_1= \theta_2=0$, $\alpha_1= \alpha_2=0$ and $\phi_1=\phi_2=0$.

At this point, it has been demonstrated that the formulation implemented can accurately model interface crack problems in transversely isotropic bimaterial.

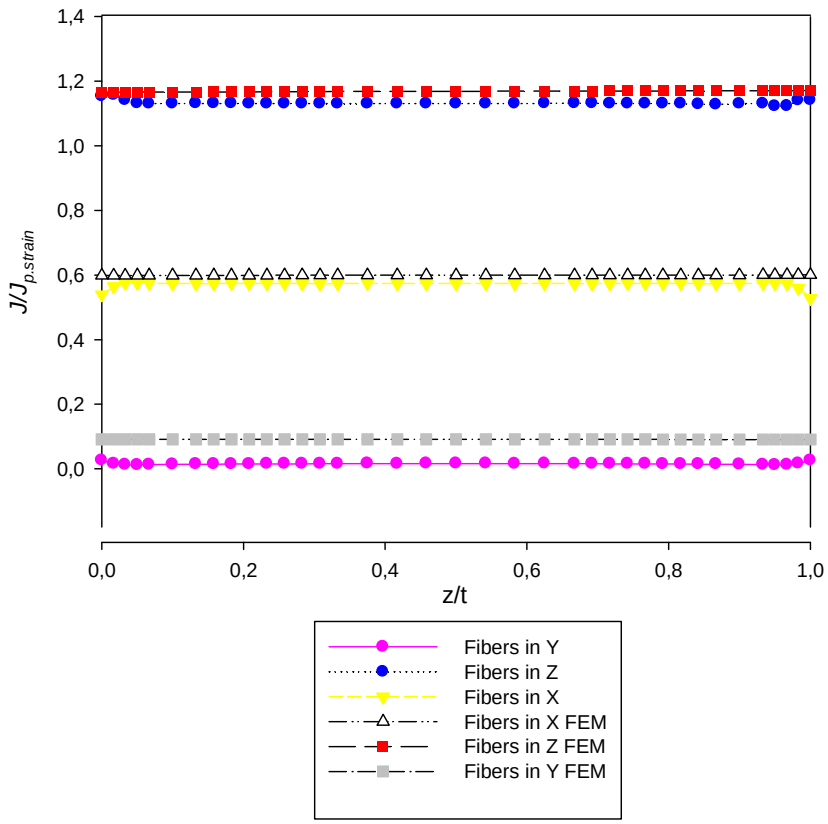

Figure 10: Variation of $J/J_{p.strain}$ with the orientation of the fibers for the thick CCP specimen

An increasingly complex problem is proposed next. Different orientations to the fibers were assigned to each of the zones of the specimen. The three-dimensional transversely isotropic bimaterial computation of the EDI along the crack front, to the author's knowledge, is not reported in the bibliography using BEM.

Table 2 indicates the director cosines for the different cases considered and Figure 11 introduces how $J/J_{p.strains}$ varies for three different cases of fiber-matrix orientation.

	Zone 1			Zone 2		
	θ_1	α_1	ϕ_1	θ_2	α_2	ϕ_2
Case 1	0	$\pi/2$	0	0	0	0
Case 2	0	$\pi/2$	0	$\pi/2$	0	0
Case 3	$\pi/4$	0	0	0	$\pi/2$	0

Table 2: Directive cosines for three different configurations of bimaterial

Consequently, in Case 1 the fibers in Zone 1 and Zone 2 are oriented in the *y*-axis and *z*-axis direction, respectively. Zone 1 in Case 2 is equal as in Case 1.However, the fibers in Zone 2 are oriented in the *x*-axis. In Case 3, the fibers of Zone 1 are pointing out a direction that forms an angle of $\theta=\pi/4$ with respect to the *z*-axis. Zone 2 fibers are oriented in *y*-axis direction.

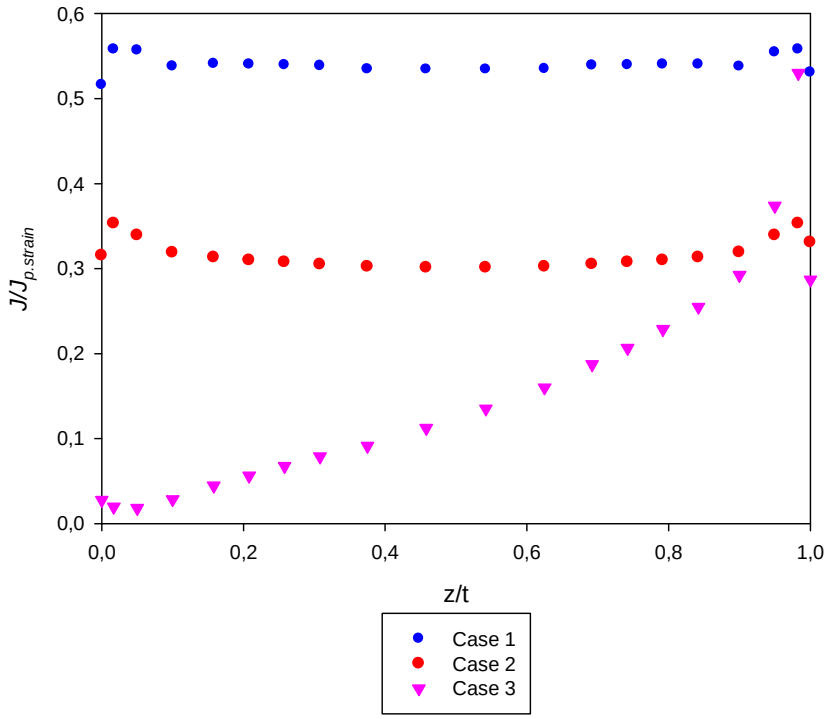

Figure 11: $J/J_{p.strain}$ along the crack front for various bimaterial configurations

Figure 11 exposes interesting results according to the relative orientation mentioned before. Case 1 and Case 2 configuration exhibits a symmetrical response along the crack front. Case 3, in contrast, shows a non-symmetrical output as a consequence of the rotation of the fibers of Zone 1 an angle of $\pi/4$ with respect to the *y*-axis.

6 CONCLUSIONS

In this paper, a boundary element analysis of three-dimensional interface cracks in transversely isotropic bimaterials has been presented. The interface crack analysis is addressed using a multidomain BEM formulation in order to account for the different material properties at both sides of the crack. The *J*-integral is computed along the crack front using the Energy Domain Integral methodology. This is implemented as a post-processing technique, and so it can be applied to the results from a particular model at a later stage. The implementation takes advantage of the efficiency of the boundary integral equation to directly obtain the required displacement derivatives, stress and strain fields from their boundary integral representations.

The devised numerical tool is employed to analyze the problem of thick centre cracked panel (CCP) under pure mode I loading in order. The CCP was submitted to many different material properties configurations and contrasted to bibliography, were it was possible, and with an ABAQUS Finite Element analysis, where the lack of references was the case.

Finally, more complex configurations were computed in order to show the versatility of the tool.

7 APPENDIX

In this appendix the fundamental solutions implemented in this code are given. These fundamental solutions, as explained above, are those of Y–C. Pan and T–W. Chou corrected by M. Loloi.

$$U_{ij}^{*} = \sum_{n=1}^{3} \alpha_n^{(ij)} F_n^{(ij)} \qquad \text{for } i,j = 1,2 \tag{A.1}$$

$$U_{i3}^{*} = \sum_{n=1}^{2} \alpha_n^{(i3)} F_n^{(i3)} \qquad \text{for } i,j = 1,2,3 \tag{A.2}$$

$$U_{ij}^{*} = U_{ji}^{*} \qquad \text{for } i,j = 1,2,3 \tag{A.3}$$

Where

$$F_3^{(11)} = \frac{1}{R_3^{*}} - \frac{d_2^{2}}{R_3 R_3^{*2}} \tag{A.4}$$

$$F_3^{(22)} = \frac{1}{R_3^{*}} - \frac{d_1^{2}}{R_3 R_3^{*2}} \tag{A.5}$$

$$F_3^{(12)} = F_3^{(21)} = \frac{d_1 d_2}{R_3 R_3^{*2}} \tag{A.6}$$

$$\alpha_3^{(ij)} = \frac{1}{4\pi \nu_3 C_{66}} \tag{A.7}$$

The rest of the functions and constants are summarized in the following tables for the cases when ν1 ≠ ν2 (Table 3) and for the degenerate case (Table 4).

Functions	Constants
$F_n^{(ij)} = \frac{\delta_{ij}}{R_n^{*}} - \frac{d_i d_j}{R_n R_n^{*2}}$	$\alpha_1^{(ij)} = -\alpha_2^{(ij)} = \frac{C_{66} - C_{33}\nu_n^{2}}{\nu_n H}$
$F_3^{(12)} = F_3^{(21)} = \frac{d_1 d_2}{R_3 R_3^{*2}}$	$\alpha_1^{(i3)} = -\alpha_2^{(i3)} = \frac{C_{13} + C_{66}}{H}$
$F_n^{(33)} = \frac{1}{R_n}$	$\alpha_1^{(33)} = -\alpha_2^{(33)} = \frac{C_{11} - C_{66}\nu_n^{2}}{\nu_n H}$

Table 3: Functions and constants in the genial formulae for fundamentals solutions of transversely isotropic materials when $\nu_1 \neq \nu_2$

Functions	Constants
$F_1^{(ij)} = \frac{\delta_{ij}}{R_1} - \frac{d_i\, d_j}{R_1^{*3}}$	$\alpha_1^{(ij)} = \frac{C_{66}\nu_1^2 - C_{11}}{\nu_1 M}$
$F_2^{(ij)} = \frac{\delta_{ij}}{R_1^{*}} - \frac{d_1^2}{R_1 R_1^{*2}}$	$\alpha_2^{(ij)} = \frac{1}{4\pi\nu_1 C_{66}}$
$F_1^{(i3)} = \frac{d_i\, d_3 \nu_1^2}{R_1^3}$	$\alpha_1^{(i3)} = \frac{\nu_1 (C_{13} - C_{66})}{M}$
$F_2^{(i3)} = 0$	$\alpha_2^{(33)} = 0$
$F_1^{(33)} = \frac{1}{R_1}$	$\alpha_1^{(33)} = \frac{\nu_1 (C_{11} + C_{66}\nu_1^2)}{M}$
$F_2^{(33)} = \frac{d_3^2 \nu_1^4}{R_1^2}$	$\alpha_2^{(33)} = -\alpha_1^{(ij)}$

Table 4: Functions and constants in the general formulae for fundamentals solutions of transversely isotropic materials for degenerate case when ν1 = ν2 (i, j=1,2)

H and M are define as follows

$$H = 4\pi C_{33} C_{66} (\nu_2^2 - \nu_1^2) \tag{A.8}$$

$$M = 8\pi C_{11} C_{66} \tag{A.9}$$

8 REFERENCES

Brebbia C.A, Telles J.L.F and Wrobel L.C. *Boundary Element Techniques*. Berlin: Springer Verlag, 1984.

Carpenter W.C., Read D.T. and Dodds R.H. *Comparison of several path independent integrals including plasticity effects*. International Journal of Fracture, 1986.

Cisilino A.P. and Aliabadi M.H. *BEM implementation of the energy domain integral for the elastoplastic analysis of 3D fracture problems*. International Journal of Fracture 1999.

Cisilino A.P. and Ortiz J.E. *Boundary Element Analysis of Three-Dimensional Mixed-Mode Cracks via the Interaction Integral*. Computer Methods in Applied Mechanics and Engineering 2004.

Cisilino A.P. and Ortiz J.E. *Boundary Element method for J-integral and stress intensity factors computations in three-dimensional interface cracks*. International Journal of Fracture, 2005.

Cisilino A.P. *Linear and Nonlinear Crack Growth using Boundary Elements*. Southampton, UK: WIT Press, 2000

Cisilino A.P., Aliabadi M.H., and Otegui J.L. *Energy domain integral applied to solve centre and double-edge crack problems in three-dimensions*. Theoretical and Applied Fracture Mechanics, 1998.

Hellen T.K. *On the method of virtual crack extensions*. International Journal of Numerical Methods in Engineering ,1975.

Loloi M. *Boundary integral equation solution of three-dimensional elastostatic problems in transversely isotropic solids using closed-form displacement fundamental solutions*. International Journal for Numerical Methods in Engineering, 2000.

Love A.E.H.A. *Treatise on the Mathematical Theory of elasticity*,1944.

Moran B. and Shih C.F.*A general treatment of crack tip contour integrals*. International Journal of Fracture, 1987.

Natha R. and Moran B. *Domain integrals for axisymmetric interface crack problems.* International Journal of Solids and Structures , 1993.

Nikishkov G.P. and Atluri S.N. *Calculation of fracture mechanics parameters for an arbitrary three-dimensional crack by the equivalent domain integral method*. International Journal of Numerical Methods in Engineering, 1987..

Pan Y.C. and Chou T.W. *Point Force Solution for an Infinite Transversely Isotropic Solid*. Journal of Applied Mechanics and Transactions,1976.

Parks D.M. *A stiffness derivative finite element technique for determination of elastic crack tip stress intensity factors*. International Journal of Fracture, 1974.

Raju I.S. and Newman J.C. *Three-dimensional finite-element analysis of finite-thickness fracture specimens*.Tech. Report NASA TN D-8414, 1977.

Rice J.R. *A path independent integral and the approximate analysis of strain concentration by notches and cracks*. ASME Journal of Applied Mechanics,1968.

Sáez A.,Ariza M.P and Dominguez J. *Three-dimensional fracture analysis in transversely isotropic solids*. Engineering Analysis with Boundary Elements Volume 20,1997.

Sáez A., Ariza M.P and Dominguez J. *Three-dimensional fracture analysis in transversely isotropic solids.* Engineering Analysis with Boundary Elements Volume 20,1997.

Saliva R., Vénere M.J., Padra C., Taroco E. and Feijoo R.A. *Shape sensitivity analysis and energy release rate of planar cracks embedded in three-dimensional bodies*. Computer Methods in Applied Mechanics and Engineering, 2000

Tada H., Paris P.C. and Irwin G.R. *The Stress Analysis of Cracks Handbook*, Third Edition, 2000.

Ting T. C. T. *Anisotropic elasticity*: *theory and Applications*, Oxford University Press, 1996